ISBN: 978-3-95450-200-4 doi:10.18429/JACoW-ICAP2018-TUPAG22

MAIN AND FRINGE FIELD COMPUTATIONS FOR THE ELECTROSTATIC QUADRUPOLES OF THE MUON *g*-2 EXPERIMENT STORAGE RING*

Eremey Valetov[1†] and Martin Berz[‡], Michigan State University, East Lansing, MI 48824, USA
[1]also at Lancaster University and the Cockcroft Institute, UK

Abstract

We consider semi-infinite electrostatic deflectors with plates of different thickness, including plates with rounded edges, and we calculate their electrostatic potential and field using conformal mappings. To validate the calculations, we compare the fringe fields of these electrostatic deflectors with fringe fields of finite electrostatic capacitors, and we extend the study to fringe fields of adjacent electrostatic deflectors with consideration of electrostatic induction, where field falloffs of semi-infinite electrostatic deflectors are slower than exponential and thus behave differently from most magnetic fringe fields. Building on the success with electrostatic deflectors, we develop a highly accurate and fully Maxwellian conformal mappings method for calculation of main fields of electrostatic particle optical elements. A remarkable advantage of this method is the possibility of rapid recalculations with geometric asymmetries and mispowered plates. We use this conformal mappings method to calculate the multipole terms of the high voltage quadrupole used in the storage ring of the Muon *g*-2 Experiment (FNAL-E-0989). Completing the methodological framework, we present a method for extracting multipole strength falloffs of a particle optical element from a set of Fourier mode falloffs. We calculate the quadrupole strength falloff and its effective field boundary (EFB) for the Muon *g*-2 quadrupole, which has explained the experimentally measured tunes, while simple estimates based on a linear model exhibited discrepancies up to 2%.

INTRODUCTION

Methods for measurement of anomalous magnetic dipole moment (MDM) and electric dipole moment (EDM) using a storage ring rely on electrostatic particle optical elements, including the Muon *g*-2 Experiment's storage ring at FNAL, which uses electrostatic quadrupoles with a curved reference orbit. Accordingly, it is necessary to accurately model main and fringe fields of electrostatic elements. In particular, inaccurate treatment of fringe fields of electrostatic elements provides a mechanism for energy conservation violation.

In this research, we address the problem of accurate representation for fringe fields of electrostatic deflectors, as well as for main and fringe fields of electrostatic quadrupoles with the specific case of the Muon *g*-2 quadrupole [1] considered. Our model of the main field of the Muon *g*-2 quadrupole allows rapid recalculations with geometric asymmetries and mispowered plates, the latter being useful, *inter alia*, for simulations of RF scraping and the effects of damaged quadrupole resistors. For the fringe field of the Muon *g*-2 quadrupole, we calculated the field map and extracted the falloff of the quadrupole strength, which was a basis for achieving a good agreement of calculated tunes with experimentally measured tunes.

CONFORMAL MAPPING METHODS

We used conformal mappings for calculation of fringe fields of electrostatic deflectors and the main field on the Muon *g*-2 quadrupole [2, App. A]. A conformal mapping (or conformal map) is a transformation $f : \mathbb{C} \to \mathbb{C}$ that is locally angle preserving. A conformal mapping satisfies Cauchy–Riemann equations and, therefore, its real and imaginary parts satisfy Laplace's equation: $\Delta\Re(f) = 0$ and $\Delta\Im(f) = 0$. Conformal mappings automatically provide the electrostatic potential in cases where the electrostatic element's geometry can be represented by a polygon, possibly with some vertices at the infinity. The domain of a conformal mapping is called the canonical domain, and the image of a conformal mapping is called the physical domain. A Schwarz–Christoffel mapping is a conformal mapping from the upper half-plane as the canonical domain to the interior of a polygon as the physical domain.

The electrostatic potential for a cross section or a longitudinal section modeled by a generalized polygon may be found by obtaining a conformal mapping f from a suitable canonical domain to the polygon. A bi-infinite strip is a suitable canonical domain if the polygon comprises two groups of consecutive sides characterized by the same constant Dirichlet boundary condition, with two constant values in total. A rectangular part of a bi-infinite strip is a suitable canonical domain when the physical domain is a logical (or generalized) quadrilateral.

If the solution of the Laplace equation in the canonical domain is ϕ, the solution of the Laplace equation in the physical domain is $\varphi = \phi \circ f^{-1}$. In practice, the electrostatic potential is usually the appropriately selected, shifted, and scaled real or imaginary part of f^{-1}.

The solution for the electrostatic potential obtained this way is fully Maxwellian in the sense that the analytic formula for f or f' results in the solution for the potential satisfying the Laplace equation.

As described in [3,4], inverse conformal mapping $g = f^{-1}$ may be obtained by

* Fermilab report FERMILAB-CONF-18-571-PPD.
† Email: evaletov@fnal.gov. ORCID: 0000-0003-4341-0379.
‡ ORCID: 0000-0001-6141-8230.

ISBN: 978-3-95450-200-4 doi:10.18429/JACoW-ICAP2018-TUPAG22

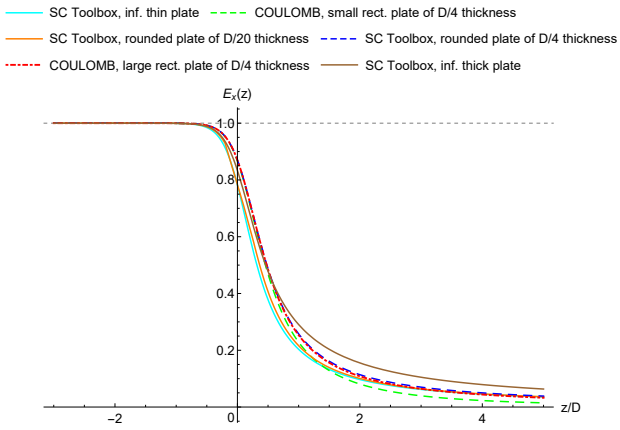

Figure 1: The electrostatic field falloffs $E_x(z)$ in cases 2 (solid cyan), 3 (solid brown), 5 (solid orange), 6 (dashed blue), 7 (dashed green), and 8 (dot-dashed red).

1. solving the equation

$$f(g(w)) - w = 0 \tag{1}$$

using the Newton–Raphson or another numerical method; or

2. solving the ODE [2, App. A]

$$\frac{dg(w)}{dw} = \frac{1}{f'(g(w))}, \quad g(w_0) = z_0. \tag{2}$$

DIFFERENTIAL ALGEBRA

The tracking code *COSY INFINITY* [5] has a rigorous and efficient implementation of differential algebra (DA) [6, pp. 86–102]. *Mathematica* also has a DA implementation, where DA values are encoded in `SeriesData` objects. One of the advantages of DA computations is that Taylor series expansions can be produced automatically for a highly complex analytic function by substituting its comprising functions with their DA values. Another advantage is the DA fixed-point algorithms, e.g., for the inversion of a Taylor series expansion, that complete in finitely many steps.

FRINGE FIELDS OF ELECTROSTATIC DEFLECTORS

Using conformal mappings, we obtained electrostatic field falloffs for semi-infinite capacitors with infinitely thin, infinitely thick, and finitely thick plates [2, Ch. 2]. For finitely thick plates, we considered plate thicknesses $D/4$ and $D/20$ in terms of the aperture D, as well as cases with rectangular and realistically rounded plate edges. The rounded edges were approximated by piecewise linear curves with 42 line segments, which is a good approximation.

In each case, we obtained a conformal mapping from the bi-infinite strip $0 \le \Im(w) \le 1$ to the physical domain of the form [3, p. 46]

$$f(w) = f(w_0) + c \int_{w_0}^{w} \exp\left[\frac{\pi}{2}(\alpha_- - \alpha_+)\zeta\right] \prod_{j=1}^{n} \left[\sinh\frac{\pi}{2}(\zeta - w_j)\right]^{\alpha_j - 1} d\zeta,$$

where the number of vertices n and angles $\pi\alpha$ are parameters of the polygonal model and the parameters w were found using the *MATLAB* package *Schwarz–Christoffel Toolbox* (*SC Toolbox*) [7].

To validate the fringe fields of semi-infinite electrostatic capacitors obtained using conformal mappings, we compared the results with the electrostatic field of finite rectangular electrostatic capacitors with finitely thick plates and different plate sizes, which were computed by Helmut Soltner (FZ Jülich) using *COULOMB*'s [8] boundary element method (BEM) field solver. This comparison shows good agreement.

Overall, the fringe fields for the following cases of one electrostatic capacitor were calculated:

1. Semi-infinite capacitor with infinitely thin plates, manually obtained conformal mapping;
2. Semi-infinite capacitor with infinitely thin plates, *SC Toolbox* calculations;
3. Semi-infinite capacitor with infinitely thick plates, *SC Toolbox* calculations;
4. Semi-infinite capacitor with plates of $D/20$ thickness, *SC Toolbox* calculations;
5. Semi-infinite capacitor with plates of $D/20$ thickness and rounded edges, *SC Toolbox* calculations;
6. Semi-infinite capacitor with plates of $D/4$ thickness and rounded edges, *SC Toolbox* calculations;
7. Large rectangular capacitor with plates of $D/4$ thickness, *COULOMB* calculations; and
8. Small rectangular capacitor with plates of $D/4$ thickness, *COULOMB* calculations.

A comparison of the fringe fields of electrostatic capacitors in cases 2–8 is shown in Fig. 1.

Because of electrostatic induction, the field of two adjacent electrostatic deflectors differs from the superposition of the fields of these deflectors as they would be in empty space. To study this effect, we modeled fringe fields of two adjacent semi-infinite capacitors with finitely thick plates and symmetric, antisymmetric, and different voltages (see Figs. 2 and 3). For adjacent electrostatic capacitors with symmetric and antisymmetric voltages, making use of the symmetries, we obtained the field using a conformal mapping from the bi-infinite strip the same way as for one electrostatic capacitor. In the case of adjacent electrostatic capacitors of different voltages, we used a composite conformal mapping that is suitable for solving the Laplace equation with multiple Dirichlet boundary conditions as detailed in [3, pp. 77–83].

We found that, unlike fringe fields of most magnetic elements, fringe fields of electrostatic deflectors fall off

ISBN: 978-3-95450-200-4 doi:10.18429/JACoW-ICAP2018-TUPAG22

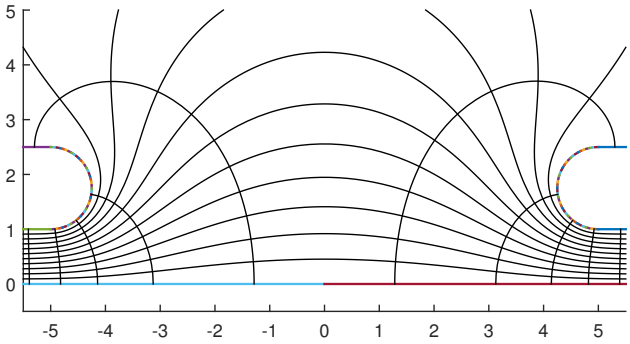

Figure 2: The electrostatic field and equipotential lines of two adjacent semi-infinite capacitors with plates of $3D/4$ thickness, symmetric voltages, and rounded edges.

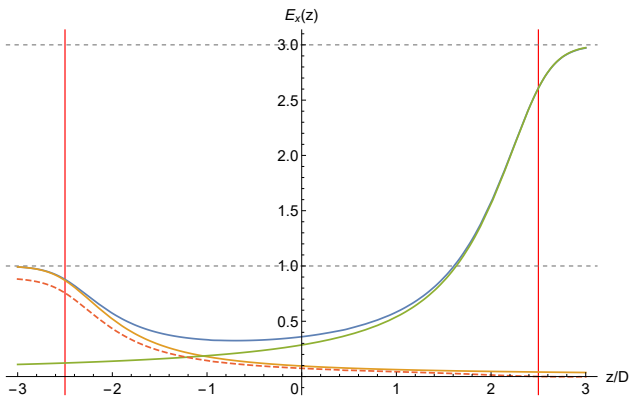

Figure 3: The electrostatic field $E_{A\&B}(z)$ (blue) of two adjacent semi-infinite capacitors with plates of $D/2$ thickness and different voltages $V_A = 1$ and $V_B = 3$, individual fields $E_A(z)$ (orange) and $E_B(z)$ (green) of each capacitor as in empty space, and the difference $E_{A\&B}(z) - E_B(z)$ (dashed red) that would be equal to $E_A(z)$ without electrostatic induction.

slower than exponentially. Thus, Enge functions of the form $F_N(z) = \left[1 + \exp\left(\sum_{j=1}^{N} a_j \left(\frac{z}{D}\right)^{j-1}\right)\right]^{-1}$, where z is the longitudinal coordinate and D is the aperture, are not suitable for accurate modeling of the asymptotic behavior of field falloffs of electrostatic deflectors, as Fig. 4 illustrates. However, a piecewise function consisting of an Enge function at $z/D < c$ and $G(z) = \left[\sum_{j=1}^{N_2} b_j \left(\frac{z}{D}\right)^{j-1}\right]^{-1}$ at $z/D \geq c$ for some $c > 0$, smoothly glued as

$$H(z) = \frac{1}{1 + \exp\left[\sum_{j=1}^{N_1} a_j \left(\frac{z}{D}\right)^{j-1}\right]} \frac{1}{1 + \exp\left[\left(\frac{z}{D} - c\right)^2\right]} + \\ + \frac{1}{\sum_{j=1}^{N_2} b_j \left(\frac{z}{D}\right)^{j-1}} \frac{1}{1 + \exp\left[-\left(\frac{z}{D} - c\right)^2\right]},$$

models field falloffs of electrostatic deflectors accurately [2, Ch. 2], as shown in Fig. 5.

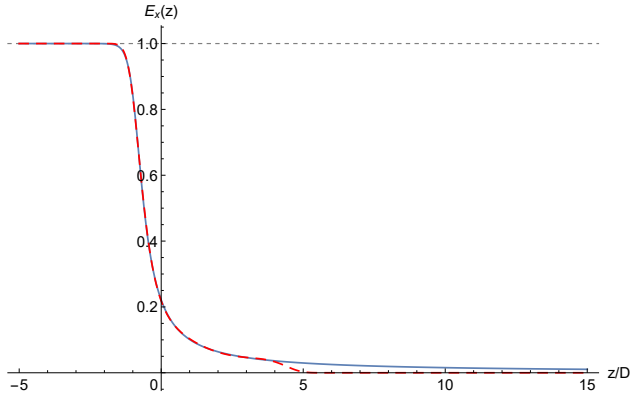

Figure 4: The plot on the left shows a 5-parameter Enge function $F_5(z)$ (dashed red), fitted to the x component of the electrostatic field falloff $E_x(z)$ (solid blue) of a semi-infinite capacitor with infinitely thin plates.

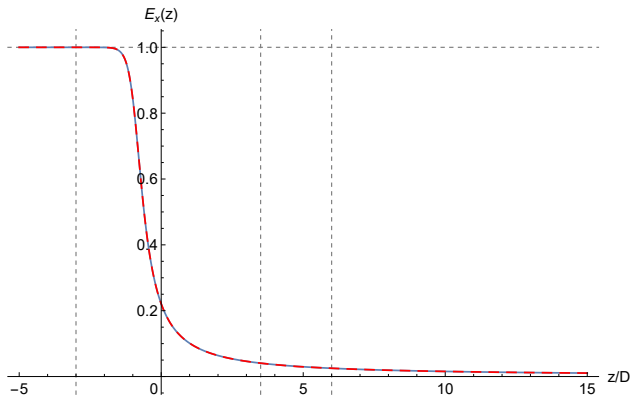

Figure 5: The plot on the right shows a function (dashed red) of the alternative form $H(z)$, fitted to $E_x(z)$ (solid blue) and enhanced in the interval $-3.5 \leq z/D \leq 6.5$ by adding a Fourier exponential series expansion of the difference $E_x(z) - H(z)$.

MAIN FIELD OF THE MUON *g*-2 COLLABORATION QUADRUPOLE

The main field of an electrostatic element such as the Muon g-2 collaboration quadrupole can be obtained using the following general method [2, 9–13]:

1. Calculate the electrostatic potential using conformal mapping methods with one plate at 1 V and the other Dirichlet boundary conditions (the remaining plates, the rectangular enclosure, and the trolley rails) of 0 V.
2. Apply plate distance errors as perturbations to four copies of the potential, each copy corresponding to one plate at 1 V and the other Dirichlet boundary conditions of 0 V.
3. Apply appropriate rotations to these four copies of the potential, scale the copies (e.g., by $\pm 2.4 \times 10^4$ or with mispowered values), and use their superposition.

We considered two polygonal models of the cross section: (1) the nominal case with symmetric voltages and no ge-

ISBN: 978-3-95450-200-4 doi:10.18429/JACoW-ICAP2018-TUPAG22

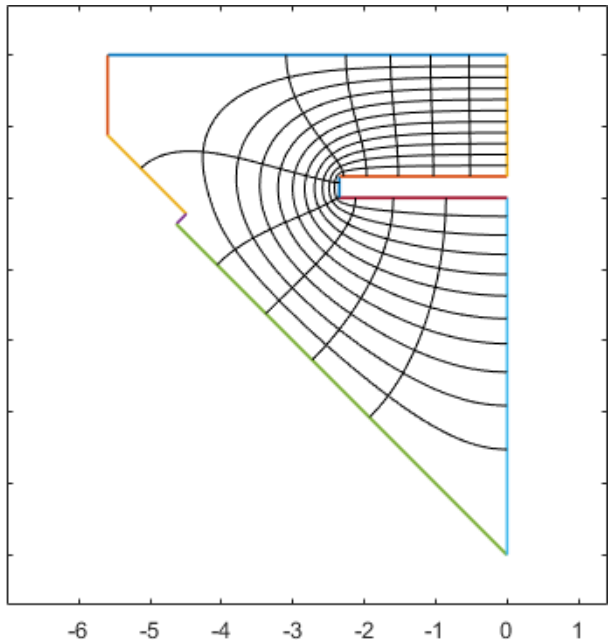

Figure 6: The polygonal model of the Muon g-2 quadrupole in the SM case.

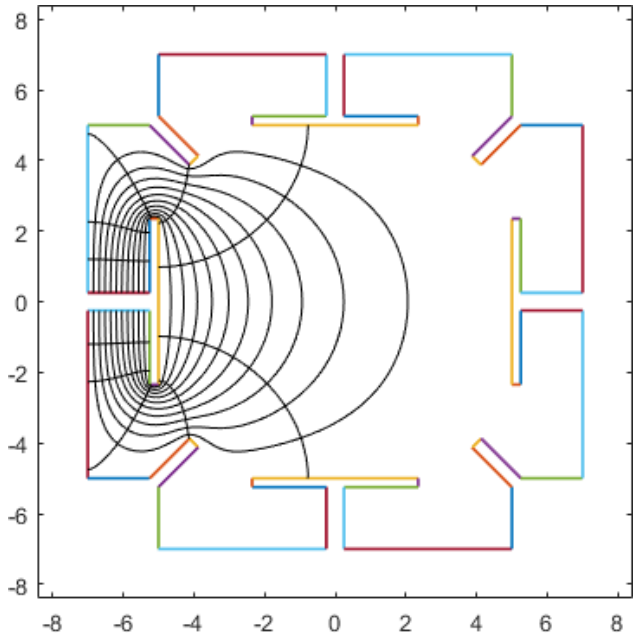

Figure 7: The polygonal model of the Muon g-2 quadrupole in the NSM case.

ometric asymmetries ("SM"), and (2) the general case of mispowered plates and geometric asymmetries ("NSM"). In the former case, we simplified the polygonal model using the four-fold rotational symmetry and the four mirror symmetries, as Fig. 6 shows. The conformal mapping theory for physical domains as n-connected regions for $n \geq 2$ is quite challenging or restricted (see, e.g., [14] and [3, pp. 64–70]) compared to simply-connected regions. We approximated the cross-sectional geometry in the NSM case by a simply-connected region shown in Fig. 7 using connecting rods between the rectangular enclosure and the four plates, which were placed in the middle of the back side of each plate to minimize their impact on the multipole terms.

In both cases, considering two constant Dirichlet boundary conditions are interposed by two von Neumann boundary conditions, forming a logical quadrilateral, we used a conformal mapping from a rectangular part of a bi-infinite strip. The derivative of the conformal map f from the canonical domain to the physical domain was [3, p. 49]

$$f'(z) = c\,\mathrm{cn}(z|m)\,\mathrm{dn}(z|m)\prod_{j=1}^{n}\left(\mathrm{sn}(z|m) - \mathrm{sn}\left(x_j + iy_j|m\right)\right)^{\alpha_j - 1},$$

where sn, cn, and dn are the Jacobi elliptic functions[1], K is the complete elliptic integral of the first kind[2], the number of vertices n and angles $\pi\alpha$ are parameters of the polygonal model, and the parameters x, y, m, and c were found using the *SC Toolbox*.

Knowing the analytic expression for a derivative f' of a conformal mapping f and the constant part (the scalar value)

$$g_0 = \mathrm{cons}(g(0)) \in \mathbb{C}$$

of the DA value of $g = f^{-1}$ at the origin $w = 0$, we can obtain the DA inverse $g(0)$ at the origin as

$$g(0) = g_0 + \left(\partial^{-1} f'(g_0)\right)^{-1}.$$

In the SM case, the derivative f' of the conformal mapping has a branch point at the preimage of the origin, which corresponds to the reference orbit. This presents certain difficulties in the analysis. For example, it is not possible to obtain the electrostatic potential multipole terms by obtaining f via a Taylor series expansion of f' and then calculating the inverse series. The same applies to the calculation of DA values of f at point $z = g_0$.

In view of this, for the SM case, we obtained the multipole expansion for the Muon g-2 quadrupole up to order 24 in the form

$$\varphi(r,\theta) = \frac{A_0}{2} + \sum_{j=1}^{N} r^j \left(A_j \cos(j\theta) + B_j \sin(j\theta)\right) + O\left(r^{N+1}\right)$$

of the electrostatic potential by solving the restriction of the ODE from Eq. (2) to the vertical edge of the polygonal model, using the solution as a boundary condition in solving the Cauchy–Riemann PDE in *Mathematica*, and performing Fourier analysis.

We also calculated the multipole expansion in *MATLAB* in the SM case up to order 24 by computing the inverse values of the conformal mapping object `f` at an equidistant discretization of a circle of radius `R` into $N = 1001$ arc intervals of length $\triangle t = 2\pi \mathtt{R}/N$ as

$$u = \left(\mathtt{f}^{-1}\left(\mathtt{R}\cos(j\triangle t), \mathtt{f}^{-1}\left(\mathtt{R}\sin(j\triangle t)\right)\right)_{j=0}^{N-1}\right),$$

[1] Definitions of the Jacobi elliptic functions can be found at `http://mathworld.wolfram.com/JacobiEllipticFunctions.html`.
[2] The complete elliptic integral of the first kind is defined at `http://mathworld.wolfram.com/CompleteEllipticIntegraloftheFirstKind.html`.

ISBN: 978-3-95450-200-4 doi:10.18429/JACoW-ICAP2018-TUPAG22

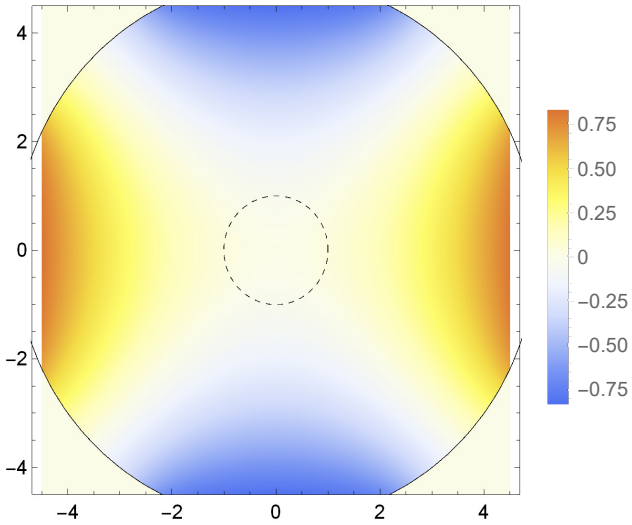

Figure 8: A heatmap plot of the multipole expansion of the electrostatic potential in the NSM case, up to order 24.

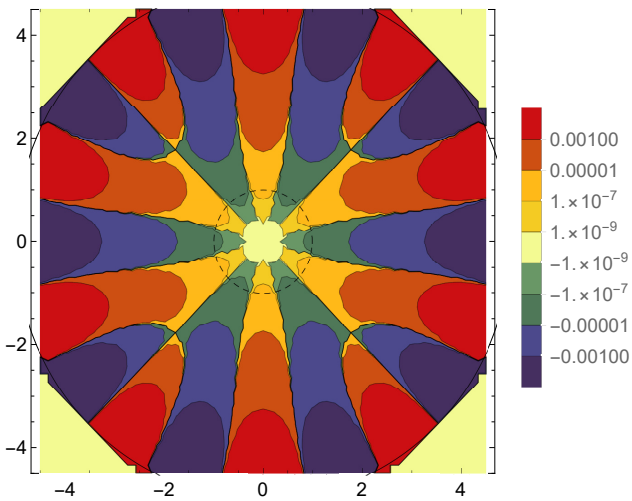

Figure 9: A contour plot of the multipole expansion of the electrostatic potential in the NSM case, orders 3 to 24.

taking the discrete Fourier transform (DFT) of the electrostatic potential φ around the circle, and obtaining the Fourier modes using the Hermitian symmetry.

For the NSM case, we obtained the multipole expansion up to order 24 using the DA inverse of the conformal mapping using *COSY INFINITY* (see Figs. 8 and 9) and *Mathematica*, as well as using Fourier analysis applied to its conventional inverse in *MATLAB*. In particular, we produced a *COSY INFINITY* program called `mterms`, as well as its variant written in *Python*, that calculates the multipole terms of the Muon g-2 quadrupole for a given set of mispowered plates and plate misalignments.

Our *a posteriori* error analysis indicates that the DA method is accurate. This application of the conformal mappings method was near its limit in terms of the complexity of geometry due to the crowding phenomenon [15], where crowding refers to a close colocation of preimages of the polygon vertices. However, the method can be expanded to significantly more complex geometries using the cross ratios of the Delaunay triangulation (CRDT) algorithm [3, 16, 17]. The conformal mappings method has the advantage of an analytic, fully Maxwellian formula and allows rapid recalculations with adjustments to the geometry and mispowered plates [2, Ch. 3].

The multipole terms we calculated for the Muon g-2 quadrupole were used to study the effects of an unpowered plate [18] and for RF scraping studies [19]. We used these multipole terms to explain the so-called oomph effect [20], which refers to the power of Muon g-2 quadrupoles being apparently 4% higher than the voltage to which they are set. More recently, the multipole terms were used to study the effect of damaged resistors with affected RC time constants on beam dynamics variables such as the beta function, tunes, and coherent betatron oscillation (CBO) frequencies in the Muon g-2 storage ring [21].

FRINGE FIELD OF THE MUON g-2 COLLABORATION QUADRUPOLE

In the fringe field of an electrostatic particle optical element, due to the dependence of the field on the longitudinal component s, the expansion of the electrostatic field takes the general Taylor–Fourier form [2, 22, 23]

$$\varphi(r,\theta,s) = \sum_{k=0}^{+\infty}\sum_{l=0}^{+\infty} M_{k,l}(s)\cos\left(l\theta+\theta_{k,l}\right) r^k.$$

Multipole terms $M_{k,l}(s)$ vanish for $k < l$ and $k = l+1, l+3, \ldots$ in the general case.

We compare it with the Fourier expansion of the electrostatic potential

$$\varphi(r,\theta,s) = \frac{a_0(r,s)}{2} + \sum_{l=0}^{+\infty} a_l(r,s)\cos\left(l\theta+\theta_l\right),$$

where we assume the constant part $a_0(r,s)/2$ to be zero, considering the gauge invariance of the electrostatic potential.

Thus, for a set of radii r_j for $j = 1, 2, \ldots, N$,

$$a_l(r_j) = \sum_{m=0}^{+\infty} M_{l+2m,l} r_j^{l+2m}, \tag{3}$$

and we can extract an approximation of the $2l$-pole strength $M_{l,l}$ from Fourier modes a_l by solving a matrix equation [23].

We developed a *Python* program called *STEP File Generator* (or `stepfg`). This program produces 3D STEP (ISO 10303-242 [24]) files from polygonal models specified by vertices. Compared to performing this process manually in CAD software, our software has workflow efficiency advantages. The resulting STEP file can be used in many general 3D, including BEM or finite element method (FEM) solver, programs.

Using the *STEP File Generator*, we effectively extruded a polygonal model of a 90° section of the full cross section of the Muon g-2 quadrupole. Due to the curvature radius $R = 711.2$ cm being relatively large compared to the half-

ISBN: 978-3-95450-200-4 doi:10.18429/JACoW-ICAP2018-TUPAG22

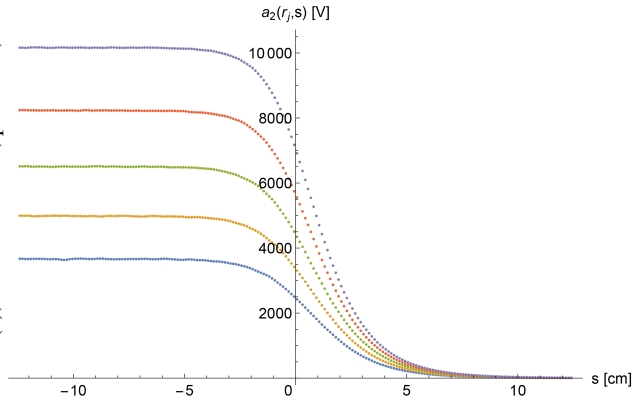

Figure 10: Falloffs of 2nd order Fourier modes $a_2\left(r_j\right)$ calculated at radii r =1.8, 2.1, 2.4, 2.7, 3.0 cm from Wu's field data. Curves with larger magnitudes correspond to larger radii.

aperture $d = 5$ cm, the approximation of a straight reference orbit is quite accurate for the purpose of calculating the fringe field.

The electrostatic potential was calculated by Helmut Soltner using *COULOMB*'s BEM field solver at a grid-point set of coordinates at a set of radii

$$r = 1.8, 2.1, 2.4, 2.7, 3.0\,\text{cm} \tag{4}$$

and longitudinal coordinates with the discretization size ranging from $\triangle z = 0.625$ cm generally to $\triangle z = 0.078$ cm near the edge of the quadrupole, where the field falloff is the steepest.

From this field data, we calculated the Fourier mode falloffs using the DFT and the Hermitian symmetry at the set of radii listed in Eq. (4). These Fourier mode falloffs are shown in Figs. 10 and 11. We extracted the quadrupole strength falloff and its effective field boundary (EFB) z_{EFB} = 1.2195 cm for the Muon g-2 quadrupole by applying the method outlined above. We also fitted Enge function coefficients using the Levenberg–Marquardt Gauss–Newton method to the falloff of the quadrupole strength [2, Ch. 3].

For a comparison, we applied [25] the same method of calculating multipole strengths to the electrostatic field data that was obtained for the Muon g-2 quadrupole using *Opera-3d*'s [26] FEM field solver by Wanwei Wu (University of Mississippi), which accounts for the curvature of the reference orbit. In particular, we interpolated Wu's field data and applied the multipole terms extraction method. Additionally, we fitted a nonlinear model defined as the multipole expansion to the raw field data in each cross section and obtained similar results. The field falloffs and the EFBs obtained from Soltner–Valetov and Wu field data are in good agreement, as Fig. 12 shows.

The discrepancies of simple estimates of the tunes based on linear models (Methods 1–3 in [27, 28]) were 1% to 2% in the case of vertical tunes, while for horizontal tunes they were 0.1% to 0.2%. In both cases, the differences between the calculated and the measured tunes exceeded the data

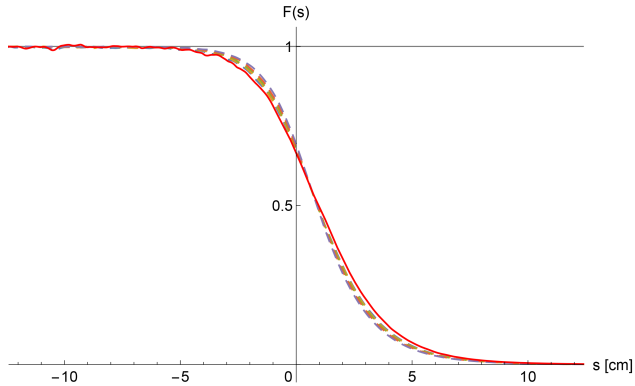

Figure 11: The Fourier modes $a_2\left(r_j\right)$ (dashed plot style, scaled to 1 well inside the quadrupole) alone fall off more quickly than the true quadrupole strength $M_{2,2}$ (solid red). This is because the second derivative of $M_{2,2}\left(s\right)$ is negative in the beginning of the fringe field and positive on the outside, impacting the additional terms based on the second derivative of $M_{2,2}$ in Eq. (3).

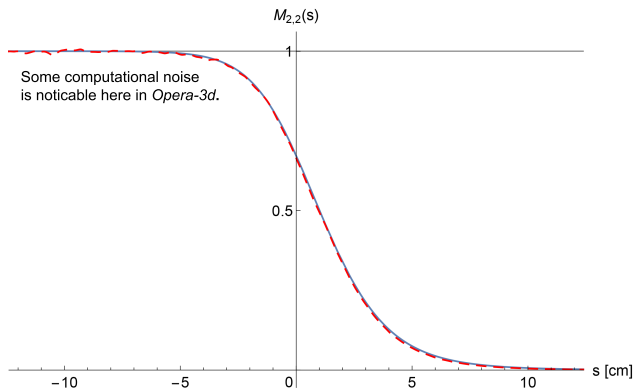

Figure 12: The falloff of the multipole term $M_{2,2}$ agrees well between calculations based on Soltner–Valetov field data (z_{EFB} = 1.2195 cm; solid blue) and field data by Wu (z_{EFB} = 1.1233 cm; dashed red).

errors of the measured tunes. The consideration of fringe fields or EFBs (Methods 5 and 4 in [27, 28], respectively) significantly improved the agreement between the calculated and the experimentally measured tunes for each quadrupole voltage. A consistency between horizontal tunes that were calculated with consideration of the fringe fields and experimentally measured tunes was reported in [29].

ACKNOWLEDGMENTS

The authors would like to acknowledge the Muon g-2 collaboration, in the context of which the work on the field of the Muon g-2 quadrupole was performed. This work was supported by the U.S. Department of Energy under Contract No. DE-FG02-08ER41546. This manuscript has been authored by Fermi Research Alliance, LLC under Contract No. DE-AC02-07CH11359 with the U.S. Department of Energy, Office of Science, Office of High Energy Physics.

ISBN: 978-3-95450-200-4 doi:10.18429/JACoW-ICAP2018-TUPAG22

REFERENCES

[1] Y. K. Semertzidis *et al.*, "The Brookhaven Muon (g-2) Storage Ring High Voltage Quadrupoles," *Nucl. Instr. Meth. Phys. Res. A*, vol. 503, no. 3, pp. 458–484, 2003.

[2] E. Valetov, "Field Modeling, Symplectic Tracking, and Spin Decoherence for EDM and Muon g-2 Lattices," Michigan State University, East Lansing, MI 48824, Ph.D. thesis, 2017, Fermilab report FERMILAB-THESIS-2017-21.

[3] T. A. Driscoll and L. N. Trefethen, *Schwarz–Christoffel Mapping*, ser. Cambridge Monographs on Applied and Computational Mathematics. Cambridge, UK: Cambridge University Press, 2002.

[4] L. N. Trefethen, "Numerical Computation of the Schwarz–Christoffel Transformation," *SIAM J. Sci. and Stat. Comput.*, vol. 1, no. 1, p. 82, 1980.

[5] K. Makino and M. Berz, "COSY INFINITY Version 9," *Nucl. Instr. Meth. Phys. Res. A*, vol. 558, no. 1, pp. 346–350, 2006. http://www.sciencedirect.com/science/article/pii/S0168900205021522

[6] M. Berz, *Modern Map Methods in Particle Beam Physics*, ser. Advances in Imaging and Electron Physics. San Diego, CA: Academic Press, 1999. [Online]. Available: https://cds.cern.ch/record/427002

[7] T. A. Driscoll, "Algorithm 756: A MATLAB Toolbox for Schwarz–Christoffel Mapping," *ACM Trans. Math. Softw.*, vol. 22, no. 2, pp. 168–186, Jun. 1996. [Online]. Available: http://doi.acm.org/10.1145/229473.229475

[8] INTEGRATED Engineering Software. *COULOMB*. https://www.integratedsoft.com/product/coulomb/.

[9] E. Valetov and M. Berz, "E989 Note 144: Main Field of the Muon g-2 Storage Ring High Voltage Quadrupole," Muon g-2 Collaboration, Fermi National Accelerator Laboratory, Batavia, IL, G-2 Experiment Document GM2-doc-11655, 2018.

[10] E. Valetov and M. Berz, "E989 Note 100: Main Field of the Muon g-2 Collaboration Quadrupole in the Case of Mispowered Plates," Muon g-2 Collaboration, Fermi National Accelerator Laboratory, Batavia, IL, G-2 Experiment Document GM2-doc-4628, 2016.

[11] E. Valetov and M. Berz, "Analytic Quad Fields Under Mispowering and Geometric Errors: March 2017 Update," Muon g-2 Collaboration, Fermi National Accelerator Laboratory, Batavia, IL, G-2 Experiment Document GM2-doc-5552, 2017.

[12] E. Valetov and M. Berz, "Potential Multipoles of the Brookhaven Muon (g-2) Storage Ring High Voltage Quadrupoles," Muon g-2 Collaboration, Fermi National Accelerator Laboratory, Batavia, IL, G-2 Experiment Document GM2-doc-4280, 2016.

[13] E. Valetov and M. Berz, "Quadrupole Multipoles from Conformal Maps, 3D Fringe Fields, and on to Full Ring Dynamics," Muon g-2 Collaboration, Fermi National Accelerator Laboratory, Batavia, IL, G-2 Experiment Document GM2-doc-3723, 2016.

[14] D. Crowdy, "The Schwarz–Christoffel Mapping to Bounded Multiply Connected Polygonal Domains," *Proc. R. Soc. A*, vol. 461, no. 2061, pp. 2653–2678, 2005.

[15] L. Banjai, Private communication.

[16] T. A. Driscoll and S. A. Vavasis, "Numerical Conformal Mapping Using Cross-Ratios and Delaunay Triangulation," *SIAM J. Sci. Comput.*, vol. 19, no. 6, pp. 1783–1803, 1998.

[17] L. Banjai, "Revisiting the Crowding Phenomenon in Schwarz–Christoffel Mapping," *SIAM J. Sci. Comput.*, vol. 30, no. 2, pp. 618–636, 2008.

[18] D. Tarazona, E. Valetov, M. Berz, and K. Makino, "Quad Plate off Scenario in Storage Ring," Muon g-2 Collaboration, Fermi National Accelerator Laboratory, Batavia, IL, G-2 Experiment Document GM2-doc-7481, 2017.

[19] D. Tarazona, M. Berz, and K. Makino, "Muon Losses - Scraping Studies COSY Update," Muon g-2 Collaboration, Fermi National Accelerator Laboratory, Batavia, IL, G-2 Experiment Document GM2-doc-8882, 2017.

[20] M. Berz, K. Makino, E. Valetov, and D. Tarazona, "Quad Voltage / Quad Voltage = Oomph: A Quantitative Oomph Theory," Muon g-2 Collaboration, Fermi National Accelerator Laboratory, Batavia, IL, G-2 Experiment Document GM2-doc-12110, 2018.

[21] D. Tarazona, M. Berz, and K. Makino, "Influence of Bad Resistors on BD Variables," Muon g-2 Collaboration, Fermi National Accelerator Laboratory, Batavia, IL, G-2 Experiment Document GM2-doc-14313, 2018.

[22] E. Valetov and M. Berz, "Fringe Field of the Muon g-2 Storage Ring High Voltage Quadrupole," Muon g-2 Collaboration, Fermi National Accelerator Laboratory, Batavia, IL, G-2 Experiment Document GM2-doc-12119, 2018.

[23] R. Jagasia, Private communication.

[24] ISO/IEC, *IS 10303-242:2014 Industrial Automation Systems and Integration – Product Data Representation and Exchange – Part 242: Application Protocol: Managed Model-Based 3D Engineering*. Geneva, Switzerland: International Organization for Standardization, 2014.

[25] E. Valetov and M. Berz, "Comparison of Field Falloffs Obtained From Two Field Datasets for the Muon (g-2) Collaboration High Voltage Quadrupole," Muon g-2 Collaboration, Fermi National Accelerator Laboratory, Batavia, IL, G-2 Experiment Document GM2-doc-7478, 2017.

[26] *OPERA-3d User Guide*. Oxford, England: Vector Fields Limited, 2004.

[27] K. Makino, E. Valetov, and M. Berz, "E989 Note 104: Detailed Linear Optics and Tunes of the g-2 Ring," Muon g-2 Collaboration, Fermi National Accelerator Laboratory, Batavia, IL, G-2 Experiment Document GM2-doc-5715, Mar. 2017.

[28] K. Makino, E. Valetov, and M. Berz, "E989 Note 110: Linear Tune Tables for the g-2 Ring," Muon g-2 Collaboration, Fermi National Accelerator Laboratory, Batavia, IL, G-2 Experiment Document GM2-doc-6791, June 2017.

[29] D. Tarazona, M. Berz, and K. Makino, "Tune/Resonances," Muon g-2 Collaboration, Fermi National Accelerator Laboratory, Batavia, IL, G-2 Experiment Document GM2-doc-12921, 2018.